Instanton calculations of tunneling splittings for water dimer and trimer

Jeremy O. Richardson, Stuart C. Althorpe, and David J. Wales

Citation: The Journal of Chemical Physics **135**, 124109 (2011); doi: 10.1063/1.3640429
View online: https://doi.org/10.1063/1.3640429
View Table of Contents: http://aip.scitation.org/toc/jcp/135/12
Published by the American Institute of Physics

Articles you may be interested in

Ring-polymer instanton method for calculating tunneling splittings
The Journal of Chemical Physics **134**, 054109 (2011); 10.1063/1.3530589

Ring-polymer molecular dynamics rate-theory in the deep-tunneling regime: Connection with semiclassical instanton theory
The Journal of Chemical Physics **131**, 214106 (2009); 10.1063/1.3267318

Quantum tunneling splittings from path-integral molecular dynamics
The Journal of Chemical Physics **144**, 114108 (2016); 10.1063/1.4943867

Semiclassical limit of quantum mechanical transition state theory for nonseparable systems
The Journal of Chemical Physics **62**, 1899 (1975); 10.1063/1.430676

Perspective: How good is DFT for water?
The Journal of Chemical Physics **144**, 130901 (2016); 10.1063/1.4944633

Derivation of instanton rate theory from first principles
The Journal of Chemical Physics **144**, 114106 (2016); 10.1063/1.4943866

PHYSICS TODAY
WHITEPAPERS

ADVANCED LIGHT CURE ADHESIVES

READ NOW

Take a closer look at what these
environmentally friendly adhesive
systems can do

PRESENTED BY
MASTERBOND
ADHESIVES | SEALANTS | COATINGS

THE JOURNAL OF CHEMICAL PHYSICS **135**, 124109 (2011)

Instanton calculations of tunneling splittings for water dimer and trimer

Jeremy O. Richardson, Stuart C. Althorpe,[a] and David J. Wales
Department of Chemistry, University of Cambridge, Lensfield Road, Cambridge, CB2 1EW, United Kingdom

(Received 15 August 2011; accepted 30 August 2011; published online 30 September 2011)

We investigate the ability of the recently developed ring-polymer instanton (RPI) method [J. O. Richardson and S. C. Althorpe, J. Chem. Phys. **134**, 054109 (2011)] to treat tunneling in water clusters. We show that the RPI method is easy to extend to treat tunneling between more than two minima, using elementary graph theory. Tests of the method on water dimer and trimer yield a set of instanton periodic orbits which correspond to all known tunneling pathways in these systems. Splitting patterns obtained from the orbits are in good overall agreement with experiment. The agreement is closer for the deuterated than for the protonated clusters, almost certainly because the main approximation in the calculations is neglect of anharmonicity perpendicular to the tunneling path. All the calculations were performed on a desktop computer, which suggests that similar calculations will be possible on much larger clusters. © *2011 American Institute of Physics*. [doi:10.1063/1.3640429]

I. INTRODUCTION

Tunneling splittings are useful observables in the study of water clusters.[1] The splittings are produced by tunneling between symmetrically equivalent permutation-inversion isomers of the global minimum.[2,3] They have been measured for clusters ranging from the dimer to the hexamer,[1,4–18] and some of these measurements have been interpreted by theory.[19–39] It is well known that water molecules behave rather differently in clusters than in the bulk. However, the properties of bulk water can often be simulated adequately using potentials that contain just pairwise and three-body terms, and the study of water clusters allows these terms to be compared more precisely and directly with experimental data than is possible in the bulk.[40–43] Tunneling splittings are particularly useful in this regard, as they are sensitive to regions of the potential energy surface away from the local minima, and thus give information on, for example, the short-range anisotropy of the potential.[40,42]

The only water cluster for which the quantum dynamics can be computed accurately is the dimer (and even then it is necessary to freeze[19–22] or separate adiabatically[23] the geometries of the monomers). However, there are a variety of methods for computing tunneling splittings that bypass direct solution of the Schrödinger equation,[24–39,44–50] some of which have been applied to water clusters.[24–30,37–39] Some of these methods are formally exact, and make use of Monte Carlo techniques;[37–39,44–47] others involve approximations, based on model Hamiltonians,[26,30] or the Wentzel-Kramers-Brillouin (WKB) approximation.[24–29,48,49] The latter approach has the advantage of yielding the splittings directly from fluctuations around a single tunneling path, but the disadvantage that the paths must be specified *a priori*. This condition requires one to develop an *a priori* model of the tunneling, which is possible for water dimer and trimer,[24–29] but more difficult for the larger clusters.[1]

An approach similar to WKB, but which does not require *a priori* specification of the tunneling path, is the "instanton" approach.[51–66] An instanton is a dominant tunneling path, obtained by analysis of the path-integral form of the quantum Boltzmann operator (or by taking the steepest-descent limit of the flux-side time-correlation function[51,52]). The use of instantons to compute tunneling splittings has a long history, but practical methods that treat multi-dimensional systems have been developed only recently, by Mil'nikov and Nakamura,[64,65] and by Richardson and Althorpe.[66] The latter "ring-polymer instanton" (RPI) method uses the "ring-polymer isomorphism" (encountered in path-integral simulations[44–47] and ring-polymer molecular dynamics[56,67–69]) to convert the abstract mathematics of formal instanton theory into a simple minimization procedure. Similar work has been done in the application of instanton theory to compute rates.[56–60] The RPI method is approximate, since it neglects anharmonicity perpendicular to the tunneling path (as do all instanton methods), and uses Cartesian coordinates, which require one to neglect the dependence of the splittings on overall rotation. It is therefore suitable for predicting dominant tunneling paths, and estimating the splittings to within an order of magnitude or better for clusters in which *a priori* prediction of the tunneling paths is difficult.

Before treating the larger clusters, it is necessary to test the RPI method on water dimer and trimer, which is the purpose of this article. We report applications of the RPI method to these systems, using *ab initio* two- and three-body potential energy surfaces recently developed by Bowman and co-workers.[22,43,70,71] (We also take the opportunity to test briefly the widely used Thole-type model potential of Ref. 41.) Water dimer can be considered to be a solved problem: its tunneling-splitting pattern is completely understood, thanks to a series of experimental measurements[4–8] and theoretical analyses.[19–26] Water trimer is less well understood, but a series of pioneering experiments[1,11–18] have yielded data on the tunneling splittings, and predictions and interpretations of these have been made by several theoretical groups.[13,27–30,37–39]

---

[a] Author to whom correspondence should be addressed. Electronic mail: sca10@cam.ac.uk.

© 2011 American Institute of Physics

To apply the RPI method to water dimer and trimer, we need to extend the theory of Ref. 66 (hereafter referred to as "Paper I") to treat tunneling between more than two minima. In Sec. II, we will show that this can be done in a straightforward way, using elementary graph theory. The RPI method then yields tunneling paths between any two permutation-inversion isomers of any local minimum, as well as the tunneling matrix and the complete splitting pattern (including the symmetry assignment of the energy levels). To our knowledge this is the first time that instanton theory has been extended in such a way. The new method is applied to the water dimer in Sec. III, and to the trimer in Sec. IV. Section V concludes the article.

II. THE RING-POLYMER INSTANTON METHOD

A. Tunneling between two symmetric wells

The RPI method was developed in Paper I to treat tunneling between two symmetrically related wells.[72] The starting point is the expression

$$\lim_{\beta\to\infty}\frac{Q(\beta)}{Q_0(\beta)}=\cosh\left(\frac{\beta\Delta}{2}\right), \tag{1}$$

where $Q(\beta)$ is the partition function of the entire system, $Q_0(\beta)$ is the partition function of the system in the absence of tunneling, $\beta = 1/\mathrm{k}T$, and Δ is the tunneling splitting, with k the Boltzmann constant.

Following the derivation of Paper I, we can calculate $Q(\beta)$ and $Q_0(\beta)$ by applying the steepest-descent approximation to the ring-polymer partition function. The latter is obtained via the well-established route of splitting the exact partition function

$$Q(\beta)=\mathrm{Tr}[\mathrm{e}^{-\beta\hat{H}}] \tag{2}$$

into N imaginary time intervals of length $\beta_N\hbar$, where $\beta_N = \beta/N$. For an f-dimensional system with potential $V(x_1,\ldots,x_f)$, this manipulation gives

$$Q(\beta)=\lim_{N\to\infty}\left(\frac{1}{2\pi\beta_N\hbar^2}\right)^{fN/2}\int \mathrm{d}\mathbf{x}\,\mathrm{e}^{-\beta_N U_N(\beta,\mathbf{x})}, \tag{3}$$

where

$$U_N(\beta,\mathbf{x})=\sum_{i=1}^{N}V(x_{i,1},\ldots,x_{i,f})+\frac{1}{2(\beta_N\hbar)^2}\times\sum_{i=1}^{N}\sum_{j=1}^{f}(x_{i+1,j}-x_{i,j})^2, \tag{4}$$

and $\{x_{1,j},\ldots,x_{N,j}\}$ are the mass-weighted polymer beads (satisfying cyclic boundary conditions) associated with the classical degree of freedom x_j.

Application of the steepest-descent approximation to the ring-polymer form of $Q_0(\beta)$ gives[66]

$$Q_0(\beta)\simeq 2\prod_{i=1}^{N}\prod_{j=1}^{f}\frac{1}{\beta_N\hbar\sqrt{\omega_i^2+\zeta_j^2}}, \tag{5}$$

where ω_i are the normal mode frequencies of the free ring-polymer, and ζ_j are the harmonic frequencies of the potential energy surface $V(x_1,\ldots,x_f)$ at the bottom of each of the two wells, where we define $V = 0$.

Application of steepest descent to the full system results in an infinite number of steepest-descent minima on the ring-polymer potential surface, which correspond to periodic orbits on the inverted (molecular) potential surface.[61–66] In each orbit, the system spends most of its time located at either one or other of the wells, but occasionally passes between them. Each pass is called a "kink," and the contribution each orbit makes to the partition function depends only on the number of kinks, n. Enumerating all such orbits, we obtain[66]

$$Q(\beta)=\sum_{n=0,\mathrm{even}}^{\infty}\frac{2N^n}{n!}Q_n(\beta), \tag{6}$$

where each term $Q_n(\beta)$ represents the contribution from an orbit with n kinks, and the prefactor is the number of ways of arranging n kinks in a ring polymer of N beads; only even values of n are included in the sum, since otherwise the orbit would not be periodic.

Fortunately, we do not need to calculate the (infinite) set of $Q_n(\beta)$ terms in Eq. (6), since each term factorises into a product of contributions made by a single, isolated kink. The latter representation is obtained by cutting an M-bead *linear* polymer out of the N-bead ring polymer, such that the ends of the linear polymer are located at the bottoms of the wells at $\mathbf{x}_\mathrm{L}$ and $\mathbf{x}_\mathrm{R}$. The potential energy surface for this linear-polymer is[66]

$$U_M(\beta,\mathbf{x})=\sum_{i=1}^{M}V(x_{i,1},\ldots,x_{i,f})+\frac{1}{2(\beta_N\hbar)^2}\sum_{j=1}^{f}\Bigg[(x_{1,j}-x_{\mathrm{L}j})^2+\sum_{i=1}^{M-1}(x_{i+1,j}-x_{i,j})^2+(x_{\mathrm{R}j}-x_{M,j})^2\Bigg]. \tag{7}$$

We then obtain a weight $\theta(\beta)$ for the contribution made by a single kink, which is given by[66]

$$\theta(\beta)=\frac{\beta_N\hbar}{\Phi}\sqrt{\frac{S_\mathrm{kink}}{2\pi\hbar}}\,\mathrm{e}^{-S_\mathrm{kink}/\hbar}, \tag{8}$$

where

$$S_\mathrm{kink}=U_M(\beta,\tilde{\mathbf{x}})\beta_N\hbar \tag{9}$$

is the classical action evaluated along the kink,

$$\Phi=\frac{\prod_{k=2}^{Nf}\eta_k}{\prod_{i=1}^{N}\prod_{j=1}^{f}\sqrt{\omega_i^2+\zeta_j^2}}, \tag{10}$$

and η_k are the frequencies of the normal modes obtained by diagonalising the Hessian corresponding to Eq. (7). Note that $\eta_1 = 0$, and that this frequency is omitted from the product. Here, ω_i are the frequencies of the free linear-polymer defined by

$$\omega_i=\frac{2}{\beta_N\hbar}\sin\frac{i\pi}{2(N+1)}, \tag{11}$$

Equation (6) can then be expressed as

$$\lim_{\beta\to\infty}\frac{Q(\beta)}{Q_0(\beta)} \simeq \lim_{\beta\to\infty}\sum_{n=0,\text{even}}\frac{N^n}{n!}\theta(\beta)^n$$
$$= \cosh[N\theta(\beta)], \tag{12}$$

and the tunneling splitting Δ is found by comparison with Eq. (1) to be

$$\Delta \simeq \lim_{\beta\to\infty}\frac{2}{\beta_N}\theta(\beta). \tag{13}$$

The main approximation in Δ is the neglect of anharmonicity perpendicular to the tunneling path. If we are to use Cartesian coordinates (which seems the only practical way of applying the approach to clusters), then we must also assume that Δ depends only weakly on the overall rotation of the system.[66] We emphasise that it is only anharmonicity *perpendicular* to the instanton tunneling-path that is neglected, and that tunneling splittings in clusters or large molecules do not usually depend strongly on the overall rotation (although there are exceptions—see Sec. III D). The RPI method can thus be expected to give an estimate of Δ, that is, good to within an order of magnitude or better for a given underlying potential energy surface.

B. Tunneling between more than two wells

We now extend the method of Paper I to treat tunneling between G degenerate wells. In place of the tunneling splitting Δ, we have a set of splittings $E_\nu - E_0$, where E_0 is the zero-point energy in the absence of tunneling, and $\nu = 1,\ 2, \ldots,\ G$. Equation (1) generalises to

$$\lim_{\beta\to\infty}\frac{Q(\beta)}{Q_0(\beta)} = \frac{1}{G}\sum_{\nu=1}^{G} e^{-\beta(E_\nu - E_0)}. \tag{14}$$

We can evaluate this expression by steepest descent, to obtain

$$Q(\beta) = \sum_{n=0,\text{even}}^{\infty}\frac{N^n}{n!}\sum_{\nu=1}^{G} Q_{n,\nu}(\beta), \tag{15}$$

where $Q_{n,\nu}(\beta)$ represents the contributions made from all periodic orbits formed from a closed sequence of n kinks that start and finish at well ν, and which have centres located at one particular set of beads $N_1 < N_2 < \ldots < N_n$ (the factor of $N^n/n!$ is the number of ways of picking this set). Each sequence of kinks joins up a different sequence of wells (starting and stopping at ν). To count the total number of sequences, we use the *adjacency matrix* $\mathbf{A}$, defined such that $A_{\lambda\mu}$ is equal to the number of possible kinks that connect well λ (directly) to well μ; when $A_{\lambda\mu} > 1$, we will assume that these kinks can be mapped onto one another by symmetry operations.[73] From elementary graph theory, the number of possible sequences of n kinks that start and end at well ν is equal to $(\mathbf{A}^n)_{\nu\nu}$.

Following the arguments given in Paper I, we can factorise the contribution to $Q_{n,\nu}(\beta)$ made by each n-kink orbit into a product of n weights, $\theta_{\lambda\mu}(\beta)$, each associated with a different kink in the sequence. The $\theta_{\lambda\mu}(\beta)$ are defined analogously to $\theta(\beta)$ in Eq. (8), such that the action $S_{\text{kink}}(\beta)$ is evaluated along the kink joining λ to μ and the ratio Φ is obtained from the normal mode frequencies of the linear polymer representing this kink, as described by Eq. (10). To obtain the total weight associated with all the n-kink orbits that contribute to $Q_{n,\nu}(\beta)$, we define the *tunneling matrix* $\mathbf{W}$ to be

$$W_{\lambda\mu} = A_{\lambda\mu}h_{\lambda\mu}, \tag{16}$$

where

$$h_{\lambda\mu} = -\lim_{\beta\to\infty}\frac{1}{\beta_N}\theta_{\lambda\mu}(\beta). \tag{17}$$

It then follows that

$$\lim_{\beta\to\infty}\frac{Q_{n,\nu}(\beta)}{Q_0(\beta)} = \frac{1}{G}[(-\beta_N\mathbf{W})^n]_{\nu\nu} \tag{18}$$

since the adjacency matrix element $A_{\lambda\mu}$ in $W_{\lambda\mu}$ ensures that the quantity $[(-\beta_N\mathbf{W})^n]_{\nu\nu}$ is the sum over the weights associated with all orbits contributing to $Q_{n,\nu}(\beta)$. We thus obtain

$$\lim_{\beta\to\infty}\frac{Q(\beta)}{Q_0(\beta)} = \frac{1}{G}\sum_{n=0,\text{even}}^{\infty}\frac{N^n}{n!}\sum_{\nu=1}^{G}[(-\beta_N\mathbf{W})^n]_{\nu\nu}$$
$$= \frac{1}{G}\text{Tr}[e^{-\beta\mathbf{W}}]. \tag{19}$$

Comparison with Eq. (14) shows that the eigenvalues of $\mathbf{W}$ are the desired approximations to the energy splittings $E_\nu - E_0$.

We can check that Eq. (19) is consistent with Eq. (12) by considering a $G = 2$ system with

$$\mathbf{A} = \begin{pmatrix} 0 & 1 \\ 1 & 0 \end{pmatrix}, \tag{20}$$

and

$$\mathbf{W} = -\frac{\theta(\beta)}{\beta_N}\mathbf{A}. \tag{21}$$

Substitution into Eq. (19) then yields Eq. (12), since $\text{Tr}(\mathbf{A}^{2n}) = 2$, and $\Delta = E_2 - E_1$. The eigenvectors of $\mathbf{W}$ are $(1, \pm 1)/\sqrt{2}$, demonstrating that the wells contribute symmetrically in the lower state, and antisymmetrically in the upper state (as expected).

For a system with $G > 2$ wells corresponding to permutation-inversion isomers, the elements of $\mathbf{W}$ related by symmetry are identical. An important first step in the application of Eq. (19) is therefore to identify the molecular symmetry group[2,3] of the system. The symmetry also determines the adjacency matrix $\mathbf{A}$ (if we assume that each element of the matrix is equal to the number of symmetrically equivalent kinks between the same pair of wells). Illustrations of these uses of symmetry are given in Secs. III and IV. A further use of symmetry is that the eigenvectors of $\mathbf{W}$ span the same irreducible representations as the corresponding wave functions (since they give the signs and magnitudes of the contributions made by the various wells), and can hence be used to assign the symmetry labels to the energy levels E_ν.

This completes the extension of the ring-polymer instanton method of Paper I to treat tunneling between more than two wells. The method is similar to the WKB approach, except for the crucial difference that the WKB approach obtains $\mathbf{W}$ from a set of *a priori* tunneling paths,[25–29] whereas the RPI method obtains $\mathbf{W}$ completely from first principles, and thus

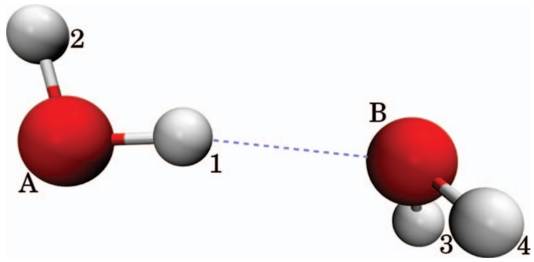

FIG. 1. Diagram showing the geometry for the local minimum corresponding to permutation-inversion isomer 1 in water dimer. The labels are used to identify the elements of the molecular symmetry group that permute the nuclei into the other seven minima. For example, (34) denotes a swap of the hydrogen atoms labelled 3 and 4, which changes the structure into that of well number 4. The water molecule containing atom "A" is referred to as the "donor;" the other water molecule is referred to as the "acceptor."

does not require an *a priori* model of the tunneling. To our knowledge, this is the first time that the instanton approach (in either its functional determinant[61–63] or ring-polymer[66] form) has been generalised to treat tunneling splittings in systems with more than two wells.

III. APPLICATION TO WATER DIMER

The newly extended RPI approach was applied to $(H_2O)_2$ and $(D_2O)_2$, using the recently developed HBB2 potential energy surface[70] (where HBB stands for Huang, Braams, and Bowman). Water dimer is an ideal test case, as the splitting pattern is non-trivial but well understood,[19–26] and the various tunneling splittings span four orders of magnitude. Also, quantum calculations on the HBB1 surface[22] (of which HBB2 is a refinement) give splitting patterns in close agreement with experiment.

A. Details of the calculation

The molecular symmetry group of water dimer[74] predicts that $\mathbf{W}$ has just five independent elements (see Sec. III B). We therefore searched for kinks between just five pairs of wells. It was straightforward to find the kinks using the technique of Paper I, whereby the linear polymer is allowed to move freely (i.e., the ends are not fixed to the wells). This approach is used because the system will typically rotate a little along the kink trajectory, and it is therefore difficult to predict *a priori* the precise start and end geometries that are joined by the kink. The initial position of the polymer was taken to be the minimum-energy path between the wells, except for one case (the 1–3 path, see below), in which the polymer was placed with half of its beads in each of the wells. In all five cases, the free polymer correctly relaxed to the kink joining the two wells in question: it was never necessary to fix the ends of the polymer to prevent it from relaxing to a kink joining a different pair of wells.

We started the searches for the kinks at relatively high temperatures (typically $\beta = 10000$ a.u.), with a relatively small number of beads (typically $M = 32$), and then increased β and M until a table of the weights $\theta_{\lambda\mu}$ versus M and β was numerically converged along the diagonal (see Paper I for examples of such tables illustrating convergence along the diagonal); β was increased in steps of 5000 a.u., and M by factors of 2, starting from $M = 32$ and finishing with $M = 4096$. When increasing M, the search was started from the geometry obtained by interpolating M beads into the minimum geometry found in the previous $M/2$ run. These values of M are typical for a system in which the tunneling does not involve a significant amount of skeletal rearrangement (and hence does not require very large numbers of beads to describe slow motion along the instanton path in the vicinity of the potential wells). All minimizations were carried out using the slightly modified L-BFGS algorithm[75,76] in OPTIM.[77] This approach has the advantage that only one matrix diagonalisation needs to be carried out per kink (in order to determine the ratio of eigenvalues Φ). Symmetry labels were assigned to the energy levels by inspecting the components of the eigenfunctions of $\mathbf{W}$.

B. Instanton tunneling paths and adjacency matrix

It is well known[26] that water dimer has $G = 8$ wells (between which it can tunnel without breaking covalent bonds). These permutation-inversion isomers are usually labelled 1–8, with the geometry of well 1 taken to be that of Figure 1. The water molecule whose hydrogen forms a hydrogen bond is called the "donor" monomer; the other monomer is the "acceptor." The geometries of the other seven wells can be generated from the geometry of well 1 by applying elements of the molecular symmetry group.[2,3] The symmetry group also predicts that there are only five independent elements of the tunneling matrix $\mathbf{W}$, which, by convention,[26] are taken to correspond to tunneling between wells 1→ i, with $i = 2, 3, 4, 5, 7$. We located a kink connecting each of these pairs of wells, following the procedure described above. Some properties of the kinks, including the computed values of h_{1i} (obtained from the linear polymers as described in Sec. II B) are given in Tables I and II. Animations, showing the motion

TABLE I. Instanton tunneling pathways (kinks) located on the HBB2 potential surface for $(H_2O)_2$. The numbers 1–8 label the eight symmetry-related wells. The permutations are defined with respect to the labels in Fig. 1. The saddle points are those that lie closest to the corresponding instanton kinks. The actions S_{kink}, eigenvalue ratios Φ, and tunneling matrix elements h_{1i} were calculated from the kinks as described in the text.

						$-h_{ij}/(\text{cm}^{-1})$	
Pathway	$i \to j$	Permutation	Saddle	$S_{\text{kink}}/(\hbar)$	$\Phi/(\text{a.u.})$	Instanton	Expt.[a]
Acceptor tunneling	1 → 4	(34)	C_s	5.74	120	5.5	2.3
Geared interchange	1 → 5	(AB)(1324)	C_i	7.48	720	0.19	0.18
Bifurcation tunneling	1 → 2	(12)(34)	C_{2v}	12.04	51	0.035	0.023
Anti-geared interchange	1 → 7	(AB)(14)(23)	C_2	11.17	140	0.029	0.013
Donor exchange	1 → 3	(12)	none	15.94	18	2.3(−3)	· · ·

[a] Reference 6.

TABLE II. Same as Table I for $(D_2O)_2$.

Pathway	$i \rightarrow j$	$S_{\text{kink}}/(\hbar)$	$\Phi/(\text{a.u.})$	$-h_{ij}/(\text{cm}^{-1})$ Instanton	$-h_{ij}/(\text{cm}^{-1})$ Expt.[a]
Acceptor tunneling	$1 \rightarrow 4$	7.75	170	0.60	0.45
Geared interchange	$1 \rightarrow 5$	10.44	900	9(−3)	9.4(−3)
Bifurcation tunneling	$1 \rightarrow 2$	16.82	67	2.7(−4)	2.3(−4)
Anti-geared interchange	$1 \rightarrow 7$	15.54	170	4(−4)	3.7(−4)
Donor exchange	$1 \rightarrow 3$	22.22	24	4(−6)	⋯

[a] Reference 5, 7, and 8.

in imaginary time of the system along each kink, are given as supplementary material.[78]

The 1–4 path is referred to as "acceptor switching" and corresponds to an exchange of atoms 3 and 4 (in the notation of Fig. 1). Previous work[24,79,80] found that this motion does not correspond to a simple internal rotation of the acceptor water but rather to a concerted twist of the donor monomer and wag of the acceptor. The computed 1–4 kink is entirely consistent with this type of motion, as can be seen from the animation. The kink differs from the minimum-energy path (used in previous WKB calculations[24–26]) in that it passes close to the second-order C_s saddle point (see Fig. 2) instead of the first-order C_1 saddle point (see Fig. 2). One effect of this difference is that there are two symmetrically equivalent kinks (between wells 1 and 4), but four symmetrically equivalent minimum-energy paths. As a result, the instanton calculations find that $A_{14} = 2$, whereas Refs. 24 and 25 use $A_{14} = 4$. This difference is only minor, because the symmetry of the C_s saddle means that the instanton paths have twice the volume in which to fluctuate about the kink, and hence the factor of two difference in A_{14} is compensated by the eigenvalue ratio Φ of Eq. (10).

The instanton predictions for the 1–5, 1–2, and 1–7 tunneling paths agree with previous work,[24,25] both in terms of the adjacency matrix (for which $A_{15} = A_{12} = A_{17} = 1$), and in terms of the tunneling dynamics along the paths (see the animations showing motion along the 1–5, 1–2, and 1–7 kinks). The most important of these paths is the 1–5 path, which corresponds to a geared interchange of the acceptor and donor monomers (see the animation). Unlike the minimum energy paths that were obtained in the previous work, the instanton paths for 1–5, 1–2, and 1–7 do not pass directly through the various saddles identified in Fig. 2, but do pass close to them.

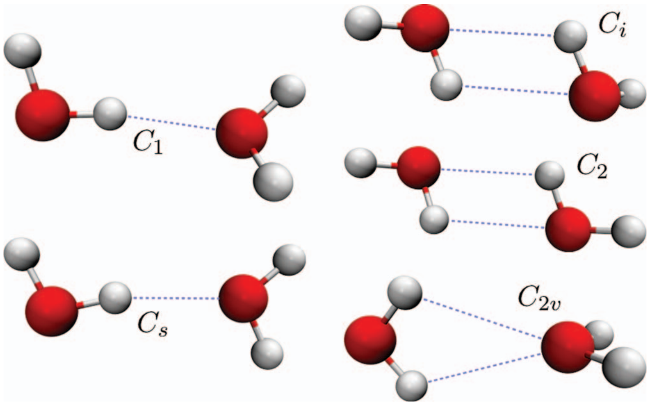

FIG. 2. Key saddle-point geometries on the HBB2 potential energy surface (Ref. 70) for water dimer. Note that the C_s saddle point is of the second order (and the others are of first order).

The remaining 1–3 path has been little studied in the literature, and is thought to contribute only a small amount to the tunneling pattern.[26] No transition state leading to wells 1 and 3 exists and so the corresponding minimum-energy path must be defined differently. Nevertheless, we were able to find an instanton kink describing this path, and obtained an adjacency matrix element $A_{13} = 4$. Unlike the other four paths, the 1–3 kink does not pass through a point with symmetry (see the animation for a visualisation of this path).

C. Tunneling matrix elements and splitting pattern

The adjacency matrix obtained from the kinks gives rise to the following tunneling matrix:

$$\mathbf{W} = \begin{pmatrix} 0 & h_{12} & 4h_{13} & 2h_{14} & h_{15} & h_{15} & h_{17} & h_{17} \\ h_{12} & 0 & 2h_{14} & 4h_{13} & h_{15} & h_{15} & h_{17} & h_{17} \\ 4h_{13} & 2h_{14} & 0 & h_{12} & h_{17} & h_{17} & h_{15} & h_{15} \\ 2h_{14} & 4h_{13} & h_{12} & 0 & h_{17} & h_{17} & h_{15} & h_{15} \\ h_{15} & h_{15} & h_{17} & h_{17} & 0 & h_{12} & 4h_{13} & 2h_{14} \\ h_{15} & h_{15} & h_{17} & h_{17} & h_{12} & 0 & 2h_{14} & 4h_{13} \\ h_{17} & h_{17} & h_{15} & h_{15} & 4h_{13} & 2h_{14} & 0 & h_{12} \\ h_{17} & h_{17} & h_{15} & h_{15} & 2h_{14} & 4h_{13} & h_{12} & 0 \end{pmatrix}. \tag{22}$$

This matrix has exactly the same form as a tunneling matrix first derived by Coudert and Hougen on the basis of a minimum-energy-path analysis,[26] and which has been widely used for describing tunneling in water dimer.[81] The minimum energy paths of Coudert and Hougen gave rise to the same adjacency matrix as the instanton kinks because they pass through the C_s saddle point, which was thought at the time to be first order. We emphasise that no reference was made to the Coudert and Hougen model when constructing $\mathbf{W}$, which was done entirely using the symmetry of the wells and kinks.

The values of the elements h_{1i}, computed from the actions $S_{\text{kink}}(\beta)$ and eigenvalue ratios $\Phi(\beta)$ are given in Tables I and II. These elements span four orders of magnitude, and it is clear that the instanton calculation has correctly predicted each of these magnitudes. Since the form of the tunneling matrix $\mathbf{W}$ is correct, it follows that instanton calculations are likely to predict the correct splitting pattern (obtained by diagonalising $\mathbf{W}$). Figure 3 and Tables III and IV show that the instanton splitting patterns agree well with experiment. Also, the symmetries of the energy levels shown in Fig. 3 (which were obtained by inspecting the eigenvectors of $\mathbf{W}$ as described above) agree with the results of variational basis set calculations.

D. Quantitative comparison with quantum results and experiment

We do not expect the RPI method to give quantitative agreement with experiment, because, as mentioned above, the

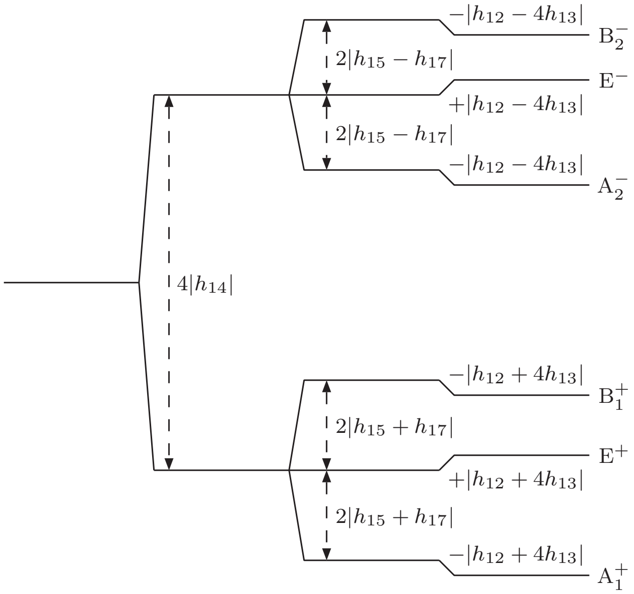

FIG. 3. Water dimer tunneling-splitting pattern, obtained by diagonalising the instanton tunneling matrix **W** of Eq. (22). The values of the tunneling elements h_{1i} and of the splittings are given in Tables I–IV.

method neglects anharmonicity perpendicular to the tunneling path, and assumes that the splittings depend only weakly on the rotational quantum numbers. Nevertheless, the agreement of the instanton results with experiment and with the quantum results of Ref. 22 is within a factor of two for $(H_2O)_2$, and even closer for $(D_2O)_2$ (although the accuracy of the latter is almost "too good" and is probably caused by fortuitous cancellation of errors).

Two pieces of evidence suggest that most of the quantitative errors in the instanton splittings result from the neglect of anharmonicity. First, the errors are a lot smaller for $(D_2O)_2$ than for $(H_2O)_2$, which are consistent with the expectation that deuteration reduces the fluctuations of the polymers around the steepest-descent minima. Second, the interchange splittings (those involving mostly h_{15}) agree much better with experiment than do the acceptor splittings. Now, the barrier height (210 cm^{-1}) along the acceptor path is close to the change in harmonic zero-point energy (204 cm^{-1}). Calculations on model systems with similarly low barriers[66] have shown that the fluctuations of a linear polymer with both ends fixed in the same well are large enough for some of the beads to access the barrier or even "visit" the other well. In such cases, $Q_0(\beta)$ is "contaminated" by tunneling, and the validity of Eq. (1) starts to break down. This effect is almost certainly why the instanton acceptor splitting is a factor of two too large in $(H_2O)_2$. Evidently this error is much smaller in $(D_2O)_2$, which is again consistent with model calculations,[66] which show a similar reduction in error on deuteration.

TABLE III. Tunneling splittings (cm^{-1}) for $(H_2O)_2$ obtained from the instanton calculations on the HBB2 surface, compared with quantum results and with experiment. See Fig. 3 for a diagram of the overall splitting pattern.

Splitting		Instanton	Quantum [a]	Expt.[b]
Acceptor	$4\|h_{14v}\|$	22	13	9.4
Interchange (lower)	$4\|h_{15}+h_{17}\|$	0.86	0.75	0.75
Interchange (upper)	$4\|h_{15}-h_{17}\|$	0.63	0.65	0.65
Bifurcation (lower)	$\|h_{12}+4h_{13}\|$	0.044	···	0.02
Bifurcation (upper)	$\|h_{12}-4h_{13}\|$	0.026	···	0.02

[a] Reference 22.
[b] Reference 6.

TABLE IV. Same as Table III for $(D_2O)_2$.

Splitting		Instanton	Quantum [a]	Expt.[b]
Acceptor	$4\|h_{14}\|$	2.4	2.4	1.8
Interchange (lower)	$4\|h_{15}+h_{17}\|$	0.037	0.040	0.039
Interchange (upper)	$4\|h_{15}-h_{17}\|$	0.035	0.036	0.036
Bifurcation (lower)	$\|h_{12}+4h_{13}\|$	2.8(−4)	···	2.3(−4)
Bifurcation (upper)	$\|h_{12}-4h_{13}\|$	2.5(−4)	···	2.2(−4)

[a] Reference 22.
[b] References 5, 7, and 8.

The instanton prediction for the acceptor splitting of $(D_2O)_2$ agrees to within 2% of the quantum result for the HBB2 potential. While this extremely close agreement is probably fortuitous, it is not unreasonable that these two results should be close. In the quantum calculations, the OH bond lengths were held fixed at their monomer equilibrium geometries, and this constraint (rather than deficiencies in the potential surface) is thought to explain the deviation from experiment.[22] The instanton calculations allow the system to relax, such that the OD distances vary correctly along the instanton path. However, Huang *et al.*[22] argue that the main error produced by fixing the OD bonds (in the quantum calculation) is neglect of zero-point energy along the tunneling path. Effectively, the instanton calculations are also neglecting a large proportion of this zero-point energy difference, through their neglect of anharmonicity. Hence both calculations make a similar approximation, and it is not surprising that the results are very close.

The values of h_{1i} are known to depend only weakly on rotational quantum numbers, except for h_{14}.[22,26] The 1–4 path involves an effective (though not actual, see above) internal twist of the two monomers, which causes h_{14} to depend strongly on the rotational quantum number K (the projection of the total rotational quantum number J onto the intermolecular axis). In Tables I and II, we have quoted the $K = 0$ experimental values for h_{14}. The instanton results may therefore include errors resulting from "contamination" from $K \neq 0$. We will not attempt to analyse these errors here, which, from the discussion above, would seem to be minor in comparison with the errors caused by the neglect of anharmonicity.

IV. APPLICATION TO WATER TRIMER

The RPI method was applied to $(H_2O)_3$ and $(D_2O)_3$, using the HBB2 potential surface[70] for two-body interactions, combined with a three-body potential;[71] [we will refer to this combination as "PES(1,2,3)"]. We also took the opportunity to test two less accurate but computationally less expensive surfaces.

A. Locating the kinks

There are 96 permutation-inversion isomers for the water trimer if covalent bonds are conserved.[14,27,28,82] Figure 4

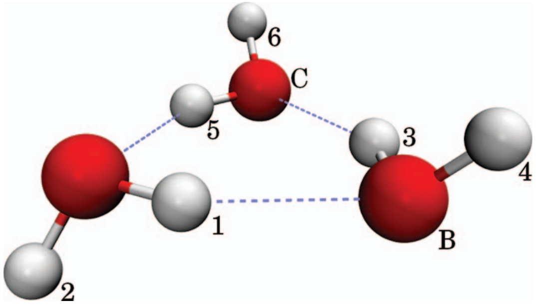

FIG. 4. Diagram showing one of the 96 minimum-energy geometries of the water trimer. The labels are used to describe operations of the G_{96} molecular symmetry group (see Ref. 14).

illustrates the geometry at the bottom of one of these wells. Each monomer acts as a single hydrogen-bond donor and single acceptor in a cyclic arrangement. The dangling hydrogens on two of the monomers point up (u) relative to the plane: these are called the "majority" monomers, and are referred to individually as the "acceptor" and the "donor," depending on their relation to the remaining "minority" monomer, in which the loose hydrogen points down (d). There are also wells with uuu and ddd geometries, but these have only a minor effect on the tunneling-splitting pattern,[14,27,28] which is dominated by tunneling between the uud wells (and the equivalent ddu, udu, etc. wells).

The permutation-inversion isomers transform into one another under operations of the G_{96} molecular symmetry group.[14,27] We ran preliminary calculations with 32 beads, at a temperature of $\beta = 15000$ a.u., to obtain a preliminary estimate of the relative importance of different kinks to the tunneling-splitting pattern. We found that many of the kinks were unimportant, because they gave tunneling matrix elements which were too small to affect the splitting pattern significantly. We identified a total of six kinks per well that made a significant contribution. These turned out to replicate qualitatively six of the major tunneling pathways that had previously been predicted for water trimer in WKB calculations.[25,27,28] These kinks were then located precisely using $M = 512$ and $\beta = 20000$ a.u. (following very similar procedures to those described in Sec. III A), and the tunneling splitting patterns were calculated using Eq. (19). The symmetry labels were very useful in assigning the levels, and were obtained by inspecting the symmetry of the eigenfunctions of $\mathbf{W}$.

B. Properties of the instanton tunneling paths

Various properties of the kinks are summarised in Table V, using the notation of Ref. 27. Conflated series of snapshots, showing the motion along each of the kinks, are shown in Fig. 5. The tunneling paths described by the kinks are qualitatively the same as those previously identified in the WKB calculations of Refs. 27 and 28 (which is why we are able to use the same notation). However, we emphasise that no prior assumptions were made about the nature of the kinks, which were found by minimizing the linear-polymer potential energy surface as described above. The resulting tunneling matrix elements for $(H_2O)_3$ and $(D_2O)_3$ are given in Table VI, and the splitting patterns in Figs. 6 and 7.

TABLE V. Instanton tunneling pathways (kinks) located on the PES(1,2,3) potential surface (Refs. 70 and 71) for $(H_2O)_3$. Properties of the kinks are summarised in the first column, using the notation of Ref. 27 for the bifurcations (min = minority monomer, don = donor monomer, acc = acceptor monomer, with the backslash separating the forward and reverse paths where these differ). The actions S_{kink} and eigenvalue ratios Φ were calculated from the kinks as described in the text.

Pathway	Shorthand	$S_{\text{kink}}/\hbar$	Φ/a.u.
Flip	Flip	2.35	300
Min + acc flip/don + min flip	A1	13.44	100
Min + don flip/acc + min flip	A2	14.85	11
Don + no flips/acc + no flips	A3	12.92	130
Min + double flip	B1	14.99	9
[Don + double flip	B2	16.13	. . .]
Acc + double flip	B3	16.57	2
Clockwise-counterclockwise	cwccw	42.93	3

1. The flip pseudorotation

Figures 6 and 7 show that the instanton splitting pattern has an overall quartet structure. This result agrees with previous experimental and theoretical studies of the trimer, in which this pattern has been shown to result from the flipping of one of the dangling hydrogens. The kink that gives rise to the overall quartet describes the flipping motion, and is shown in Fig. 5(a).

Interestingly, the flip does not involve tunneling, since the zero-point energy in the wells is slightly greater (by 27 cm^{-1}) than the barrier height. For this reason, the flip is often regarded as a torsional vibration,[14] and is assigned pseudorotational quantum numbers $k = 0, \pm 1, \pm 2, 3$. Nevertheless, the instanton splitting agrees with experiment to within a factor of 2.3 for $(H_2O)_3$ and 1.8 for $(D_2O)_3$. This relatively good agreement should come as no surprise, since Eq. (14) is clearly applicable to the flipping motion, provided one can define a $Q_0(\beta)$ from which paths that flip onto or over the barrier are excluded. The ability of the instanton approach to describe the flip is thus very similar to its ability to describe the acceptor tunneling in water dimer (see Sec. III D), for which the zero-point energy of the wells is slightly below the barrier. In fact, there is no clear distinction between these two types of process: they will both contain significant errors arising from the neglect of anharmonicity, because paths that have both ends fixed in one well can describe fluctuations onto or over the barrier. The relatively good

TABLE VI. Instanton tunneling elements $-h_{ij}$ (cm^{-1}), calculated for $(H_2O)_3$ and $(D_2O)_3$ using the PES(1,2,3) (Refs. 70 and 71), PES(1,2,KS/WB) (Ref. 43) and TTM3-F (Ref. 41) surfaces.

	$(H_2O)_3$			$(D_2O)_3$
Pathway	PES(1,2,3)	PES(1,2,KS/WB)	TTM3-F	PES(1,2,3)
Flip	50	60	47	18
A1	0.005	0.007	0.0019	2.0(−5)
A2	0.011	0.02	0.0024	3.1(−5)
A3	0.006	0.007	0.0010	3.5(−5)
B1	0.011	0.02	0.0053	3.0(−5)
B3	0.009	0.02	0.0055	1.7(−5)
cwccw	5(−14)	2(−13)	1.1(−13)	5.6(−21)

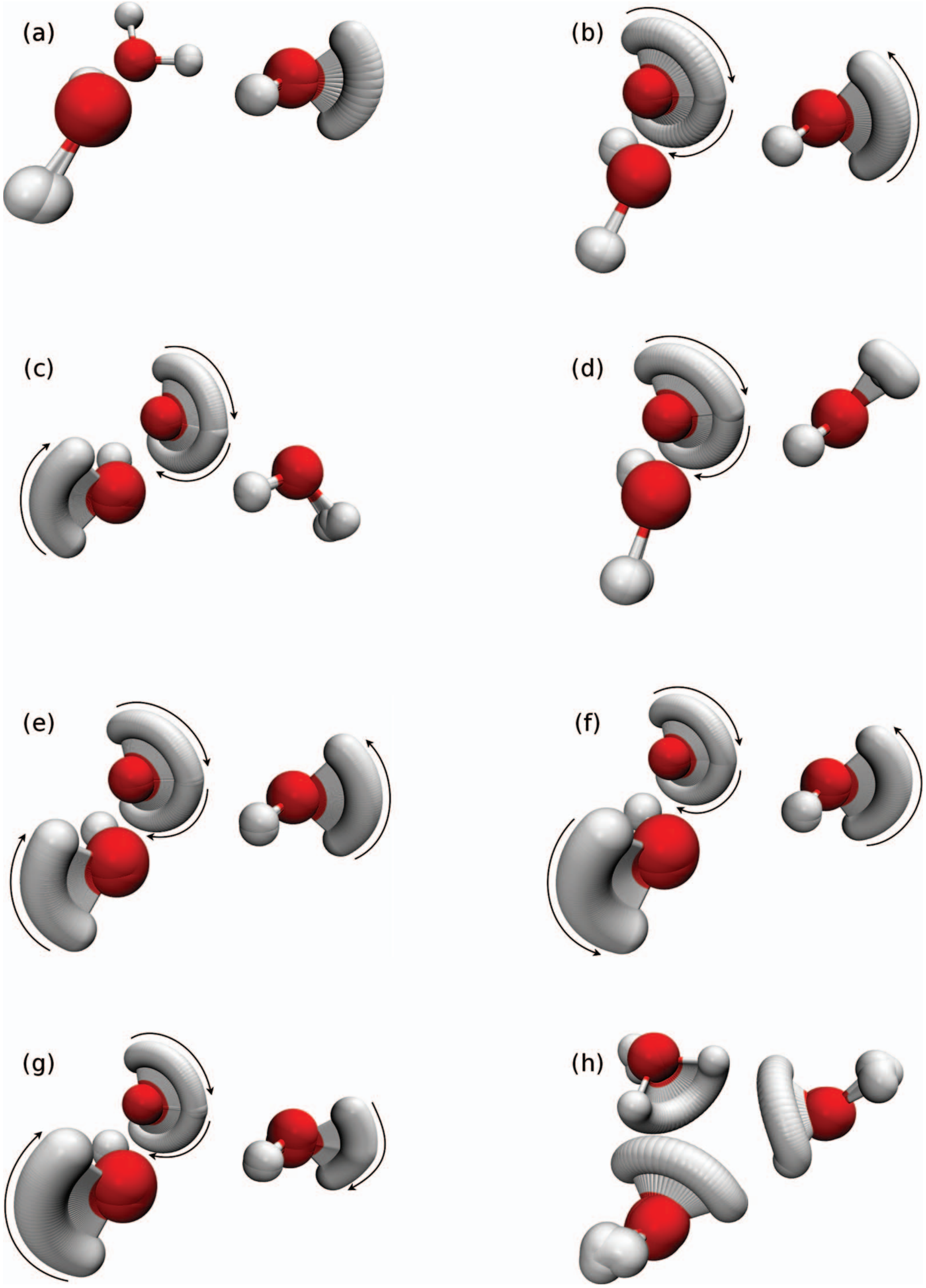

FIG. 5. Conflated snapshots of instanton tunneling paths (kinks) obtained using the PES(1,2,3) surface (Refs. 70 and 71) for $(H_2O)_3$. The paths shown are (a) the flip, (b)–(g) the A1, A2, A3, B1, B2, and B3 bifurcations, and (h) the cwccw path. The arrows show the direction of motion of the hydrogen atoms. Note that the B2 path (f) does not contribute to the tunneling because it is a saddle-point on the linear polymer surface (see text).

agreement of the flip with experiment indicates that only a small proportion of the paths in $Q_0(\beta)$ manage to reach or cross the barrier. There would be a larger proportion of such paths if the flips were more facile, which would lead to a breakdown of the instanton approximation.

2. Bifurcation tunneling

The more detailed structure in the instanton splitting patterns (Figs. 6 and 7) is produced by the kinks labelled A1, A2, A3, B1, and B3 (see Fig. 5 and Table V). Each of these kinks gives the same qualitative description of the tunneling as one of the paths identified in previous WKB calculations[27,28] (from where we have taken the notation). These paths describe "bifurcation tunneling," meaning that the dangling hydrogen on one of the monomers swaps roles with the bonding hydrogen, such that the geometry of the cluster passes through a bifurcated structure.[82] These "bifurcation" paths differ in the number of accompanying flips (see Fig. 5 and Table V), and in

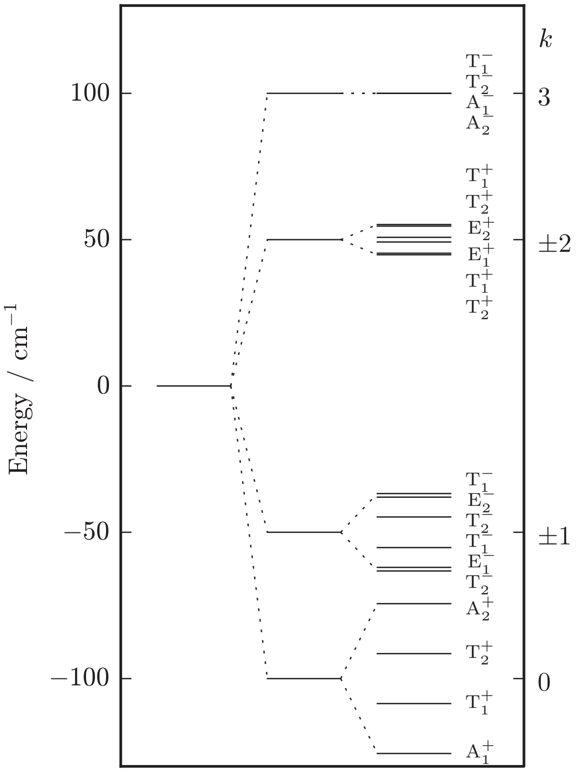

FIG. 6. Tunneling-splitting pattern for $(H_2O)_3$, obtained by diagonalising the instanton tunneling matrix **W** of Eq. (22). The first set of lines is unscaled, and only the overall quartet splitting produced by the flip is visible. Magnification by a factor of 400 produces the second set of lines, which show the bifurcation splitting pattern. The values of the tunneling elements h_{1i} are given in Table VI. There is an accidental degeneracy for the $k = 3$ levels which disappears within the numerical errors of the calculation. The energy levels used to plot this figure are tabulated in the supplementary material (Ref. 78).

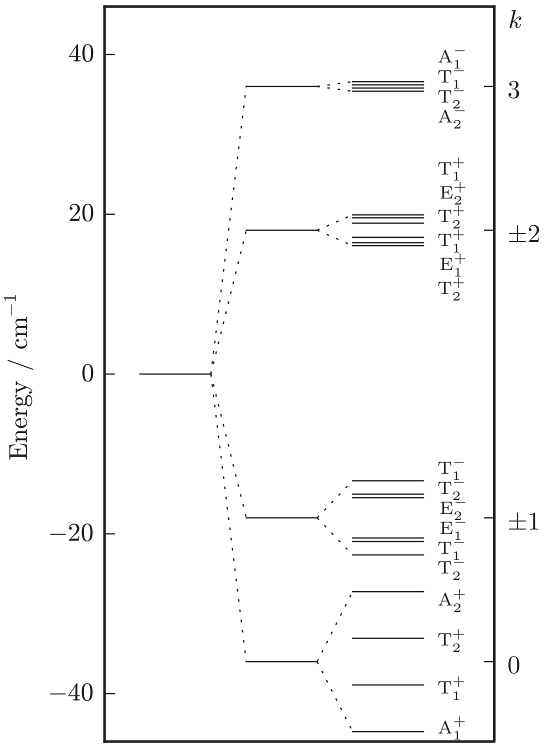

FIG. 7. Same as Fig. 6 for $(D_2O)_3$. The second set of lines showing the bifurcation splittings have been magnified by a factor of 40000.

whether the path is self-reversible, i.e., whether the monomers have the same roles within the cluster at the start and finish of the path (which is true only of the "B" paths).

The contributions of the various bifurcation kinks to the splitting pattern are difficult to disentangle, and we will not attempt a detailed analysis here. Tables V and VI show that the actions of these paths differ significantly, but that these differences are roughly compensated by changes in the values of the eigenvalue ratio Φ of Eq. (10). As a result, the five bifurcation paths make contributions to the splitting pattern of roughly equal importance. We will return to this point in Sec. IV C below.

Previous WKB calculations[27,28] identified an additional bifurcation path, denoted by B2. There is in fact a stationary point corresponding to B2 on the linear polymer surface (see Fig. 5(f) and Table V), but it is a first-order saddle: linear polymers set to this geometry relax into combinations of the flip and the A1 path. As a result, semiclassical tunneling between the wells connected by the B2 path proceeds via combinations of the flip and A1; *not* via B2. We therefore set the corresponding elements of **W** to zero. No changes needed to be made to incorporate the combined flip and A1 paths, since the flip and A1 are already included individually in **W**, and the treatment of Sec. II B ensures that all possible combinations of individual paths are included in $Q(\beta)$. We note that the other potential energy surfaces tested (see Sec. IV D) also returned first-order saddles for the linear polymer corresponding to B2, so we can be quite confident that the B2 path does not contribute significantly to the splitting pattern in water trimer.

3. *Clockwise-counterclockwise tunneling*

No combination of the six instanton paths described above is able to convert a minimum-energy geometry of water trimer into the permutation-inversion isomer corresponding to reversal of the hydrogen-bonding pattern in the ring in Figure 4. The corresponding generator operation is (35)(46)(BC)*. As a result, the tunneling can be classified using the G_{48} molecular symmetry group instead of G_{96},[27,82] and the wells split into two sets, which are not coupled by **W**. This finding is consistent with all recent studies of the water trimer,[14] in which tunneling between these subsets is thought not to contribute to the splitting patterns.

Nevertheless, the possibility of a tunneling path corresponding to this generator in water trimer has been discussed in the literature,[14,29] and we thought that it would be a good test of the instanton method to see whether it is capable of finding such a path. The corresponding mechanism is a concerted breaking and reforming of all three of the hydrogen bonds, in a motion described as "clockwise-counterclockwise" (cwccw) tunneling.[14] It was straightforward to locate the cwccw kink, which is shown in Fig. 5(h). As expected, the action of this kink is very large (Table V), and the tunneling matrix element negligibly small (Table VI).

C. Comparison of splitting patterns with experiment

The instanton splitting patterns of Figs. 6 and 7 are in good overall agreement with the results of experiment,[1,11–18] in which far infrared spectra for $(H_2O)_3$ and $(D_2O)_3$ have been interpreted in terms of an overall quartet structure caused by the flip pseudorotation, each branch of which is further split by bifurcation tunneling. The latter gives rise to quartets in the spectrum, which are either equally spaced or "anomalous".[13,14] The former are associated with the outer $k = 0, 3$ branches; the latter with the $k = \pm 1, \pm 2$ inner branches (for rotational quantum number $K = 0$). This is consistent with Figs. 6 and 7, provided one assumes that the inner sextets give rise to what appear to be unevenly spaced quartets in the spectrum.

A more detailed comparison with experiment is difficult for the trimer, owing to complexities in the rovibrational spectrum caused by, among other things, a dependence of the $k = \pm 1, \pm 2$ bifurcation splitting pattern on Coriolis coupling.[13,14] As mentioned above, the RPI method assumes that dependence of the splitting on overall rotation can be neglected. The effects of rotational coupling are much weaker here than in the water dimer accepter splitting (see Sec. III D), but details of the $k = \pm 1, \pm 2$ bifurcation splitting pattern are sensitive to small changes in the elements h_{ij}, since the pattern results from the interplay of several competing paths of roughly equal weight. An attempt to replicate this pattern in detail would therefore go beyond the capabilities of the instanton method.

One property, however, which the instanton approach should be able to describe is the overall dependence of the bifurcation splitting on k. The instanton calculations predict that this splitting decreases markedly with increase in k (see Figs. 6 and 7). However, a recent analysis[13] of the experimental spectrum predicts that the bifurcation splitting is roughly k-independent. This disagreement arises because the instanton calculations predict that all five of the bifurcation tunneling paths contribute roughly equally to the splitting (see Table VI), whereas Ref. 13 finds that the B2 path dominates. It might be that neglect of anharmonicity causes the instanton method to overestimate the contributions made by some of the other bifurcation paths, or that alternative analyses of the experimental data are possible that are consistent with Figs. 6 and 7. Further work will be needed to resolve this assignment.

Table VII gives numerical comparisons of the instanton tunneling splittings with experiment and with the results of previous Diffusion Monte Carlo (DMC) (Refs. 37 and 38) and WKB (Ref. 28) calculations. Comparison of the flip splittings is straightforward, but comparison of the bifurcation splittings requires us to take into account the variation with k, which is present in the instanton results but is not found in the analysis of Ref. 13 (see above). Table VI gives the instanton bifurcation splittings corresponding to the $k = 0$ quartet which is probably also where the experimental results are measured. Note that the DMC and WKB results were also obtained under the assumption that the bifurcation splitting does not vary strongly with k, and used potential energy surfaces that were not as accurate as PES(1,2,3).

TABLE VII. Tunneling splittings (cm^{-1}), obtained from the instanton calculations, from previous DMC (Ref. 37) and WKB (Ref. 28) calculations, and from experiment (Refs. 13 and 14). The comparison of the bifurcation splittings is intended only as a rough guide (see text).

Pathway	Instanton	DMC	WKB	Expt.
$(H_2O)_3$ flip	100	22	37.93	43.52
$(D_2O)_3$ flip	36	9	30.84	20.54
$(H_2O)_3$ bifurcation	4.3(−2)	1.7(−2)	6.50(−3)	9.63(−3)
$(D_2O)_3$ bifurcation	1.4(−4)	4.0(−3)	2.54(−5)	1.66(−4)

D. Comparison between different potential energy surfaces

We also took the opportunity to compare tunneling splittings obtained from two less accurate (but computationally cheaper) potential energy surfaces with those obtained using PES(1,2,3). Table VII gives the values of h_{ij} calculated using the PES(1,2,KS/WB) surface[43] and the Thole-type model TTM3-F surface.[41]

The PES(1,2,KS/WB) surface includes an efficient three-body potential, which was obtained by refitting the *ab initio* points used to generate PES(1,2,KS/WB) to an approximate form derived by Kumar and Skinner.[83] The PES(1,2,KS/WB) surface gives an adequate description of the tunneling in water trimer, yielding values of h_{ij} that are within a factor of two of those obtained using PES(1,2,3).

The TTM3-F surface is designed to be inexpensive to evaluate the simulations of liquid water, and cannot realistically be expected to compete with PES(1,2,3) in accuracy. Nevertheless, this surface gives qualitatively the same prediction of the tunneling dynamics as PES(1,2,3), yielding the same set of instanton paths as those shown in Fig. 5 (including the B2 path, which is a first-order saddle on the linear polymer surface, as for the other two surfaces), and yielding splitting patterns with the same overall structure as Figs. 6 and 7. The splittings disagree with those obtained from PES(1,2,3) by at most a factor of 6 (Table VI).

V. CONCLUSIONS

We have extended the RPI method of Paper I to treat tunneling between more than two symmetry-related minima, and have tested the ability of the approach to treat tunneling in water clusters by applying it to water dimer and trimer. The results are extremely promising, showing that the instanton method gives a good overall description of the tunneling. In particular, it was straightforward to locate instanton kinks (sections of periodic orbits) describing all of the main tunneling pathways in both the dimer and the trimer. The kinks described the same tunneling mechanisms as those obtained in the previous calculations, and the obtained splitting patterns are in good overall agreement with the experiment. We should emphasise that no prior assumptions needed to be made about the nature of the instanton tunneling paths, which were determined entirely by minimizing linear polymers, using the technique of Paper I.

The instanton method is approximate, and it would be unwise to expect it to yield quantitative agreement with experiment, or to predict exactly the fine details of complex splitting patterns such as the bifurcation splitting in water trimer. The acceptor splitting in water dimer was overestimated (by a factor of two), as was the splitting caused by the flip in water trimer. These errors were almost certainly caused by the neglect of anharmonicity perpendicular to the tunneling path. This error is always present in instanton calculations, although the crucial anharmonicity *along* the path is included correctly. As a result, the instanton method can be expected to yield closer numerical agreement with experiment for a fully deuterated rather than a fully protonated cluster.

All the calculations reported in this article were carried out in a few days on a desktop computer. The approach is easy to parallelise (since the polymer beads can be distributed onto different computer nodes) and hence should be straightforward to scale up to treat tunneling in larger water clusters, about which much remains to be learnt.

ACKNOWLEDGMENTS

We thank Y. Wang and J. M. Bowman for supplying their potential energy subroutines. J.O.R. acknowledges a Doctoral Training Account Ph.D. studentship from the UK Engineering and Physical Sciences Research Council.

[1] F. N. Keutsch and R. J. Saykally, Proc. Natl. Acad. Sci. U.S.A. **98**, 10533 (2001).
[2] H. C. Longuet-Higgins, Mol. Phys. **6**, 445 (1963).
[3] P. R. Bunker and Per Jensen, *Molecular Symmetry and Spectroscopy*, 2nd ed. (NRC Research Press, Ottawa, 1998).
[4] G. T. Fraser, R. D. Suenram, and L. H. Coudert, J. Chem. Phys. **90**, 6077 (1989).
[5] R. D. Suenram, G. T. Fraser, and F. J. Lovas, J. Mol. Spectrosc. **138**, 440 (1989).
[6] E. Zwart, J. J. ter Meulen, W. Leo Meerts, and L. Coudert, J. Mol. Spectrosc. **147**, 27 (1991).
[7] E. N. Karyakin, G. T. Fraser, and R. D. Suenram, Mol. Phys. **78**, 1179 (1993).
[8] J. B. Paul, R. A. Provencal, and R. J. Saykally, J. Phys. Chem. A **102**, 3279 (1998).
[9] L. B. Braly, J. D. Cruzan, K. Liu, R. S. Fellers, and R. J. Saykally, J. Chem. Phys. **112**, 10293 (2000).
[10] L. B. Braly, K. Liu, M. G. Brown, F. N. Keutsch, R. S. Fellers, and R. J. Saykally, J. Chem. Phys. **112**, 10314 (2000).
[11] N. Pugliano and R. J. Saykally, Science **257**, 1937 (1992).
[12] K. Liu, J. G. Loeser, M. J. Elrod, B. C. Host, J. A. Rzepiela, N. Pugliano, and R. J. Saykally, J. Am. Chem. Soc. **116**, 3507 (1994).
[13] F. N. Keutsch, R. J. Saykally, and D. J. Wales, J. Chem. Phys. **117**, 8823 (2002).
[14] F. N. Keutsch, J. D. Cruzan, and R. J. Saykally, Chem. Rev. **103**, 2533 (2003).
[15] M. R. Viant, J. D. Cruzan, D. D. Lucas, M. G. Brown, K. Liu, and R. J. Saykally, J. Phys. Chem. A **101**, 9032 (1997).
[16] K. Liu, M. G. Brown, M. R. Viant, J. D. Cruzan, and R. J. Saykally, Mol. Phys. **89**, 1373 (1996).
[17] E. H. T. Olthof, A. van der Avoird, P. E. S. Wormer, K. Liu, and R. J. Saykally, J. Chem. Phys. **105**, 8051 (1996).
[18] S. Suzuki and G. A. Blake, Chem. Phys. Lett. **229**, 499 (1994).
[19] S. C. Althorpe and D. C. Clary, J. Chem. Phys. **101**, 3603 (1994).
[20] S. C. Althorpe and D. C. Clary, J. Chem. Phys. **102**, 4390 (1995).
[21] H. Chen, S. Liu, and J. C. Light, J. Chem. Phys. **110**, 168 (1999).
[22] X. Huang, B. J. Braams, J. M. Bowman, R. E. A. Kelly, J. Tennyson, G. C. Groenenboom, and A. van der Avoird, J. Chem. Phys. **128**, 034312 (2008).
[23] C. Leforestier, F. Gatti, R. S. Fellers, and R. J. Saykally, J. Chem. Phys. **117**, 8710 (2002).
[24] T. Taketsugu and D. J. Wales, Mol. Phys. **100**, 2793 (2002).
[25] Y. Watanabe, T. Taketsugu, and D. J. Wales, J. Chem. Phys. **120**, 5993 (2004).
[26] L. H. Coudert and J. T. Hougen, J. Mol. Spectrosc. **130**, 86 (1988).
[27] T. R. Walsh and D. J. Wales, J. Chem. Soc., Faraday Trans. **92**, 2505 (1996).
[28] M. Takahashi, Y. Watanabe, T. Taketsugu, and D. J. Wales, J. Chem. Phys. **123**, 044302 (2005).
[29] T. Loerting, K. R. Liedl, and B. M. Rode, J. Chem. Phys. **109**, 2672 (1998).
[30] A. van der Avoird, E. H. T. Olthof, and P. E. S. Wormer, J. Chem. Phys. **105**, 8034 (1996).
[31] D. Sabo, Z. Bačić, T. Bürgi, and S. Leutwyler, Chem. Phys. Lett. **244**, 283 (1995).
[32] W. Klopper and M. Schütz, Chem. Phys. Lett. **237**, 536 (1995).
[33] D. Sabo, Z. Bačić, S. Graf, and S. Leutwyler, Chem. Phys. Lett. **261**, 318 (1996).
[34] D. Sabo, Z. Bačić, S. Graf, and S. Leutwyler, J. Chem. Phys. **110**, 5745 (1999).
[35] D. Sabo, Z. Bačić, S. Graf, and S. Leutwyler, J. Chem. Phys. **111**, 5331 (1999).
[36] D. Sabo, Z. Bačić, S. Graf and S. Leutwyler, J. Chem. Phys. **111**, 10727 (1999).
[37] J. K. Gregory and D. C. Clary, J. Chem. Phys. **102**, 7817 (1995).
[38] J. K. Gregory and D. C. Clary, J. Chem. Phys. **103**, 8924 (1995).
[39] D. Blume and K. B. Whaley, J. Chem. Phys. **112**, 2218 (2000).
[40] R. Bukowski, K. Szalewicz, G. C. Groenenboom, and A. van der Avoird, Science **315**, 1249 (2007).
[41] G. S. Fanourgakis and S. S. Xantheas, J. Chem. Phys. **128**, 074506 (2008).
[42] K. Szalewicz, C. Leforestier, and A. van der Avoird, Chem. Phys. Lett. **482**, 1 (2009).
[43] Y. Wang and J. M. Bowman, Chem. Phys. Lett. **491**, 1 (2010).
[44] A. Kuki and P. G. Wolynes, Science **236**, 1647 (1987).
[45] D. M. Ceperley and G. Jacucci, Phys. Rev. Lett. **58**, 1648 (1987).
[46] C. Alexandrou and J. W. Negele, Phys. Rev. C **37**, 1513 (1988).
[47] M. Marchi and D. Chandler, J. Chem. Phys. **95**, 889 (1991).
[48] W. H. Miller, J. Phys. Chem. **83**, 960 (1979).
[49] N. Makri and W. H. Miller, J. Chem. Phys. **91**, 4026 (1989).
[50] M. Ben-Nun and T. J. Martínez, J. Phys. Chem. A **103**, 6055 (1999).
[51] W. H. Miller, J. Chem. Phys. **62**, 1899 (1975).
[52] S. C. Althorpe, J. Chem. Phys. **134**, 114104 (2011).
[53] C. G. Callan and S. Coleman, Phys. Rev. D **16**, 1762 (1977).
[54] J. Cao and G. A. Voth, J. Chem. Phys. **105**, 6856 (1996).
[55] Z. Smedarchina, W. Siebrand, and A. Fernández-Ramos, J. Chem. Phys. **127**, 174513 (2007).
[56] J. O. Richardson and S. C. Althorpe, J. Chem. Phys. **131**, 214106 (2009).
[57] S. Andersson, G. Nyman, A. Arnaldsson, U. Manthe, and H. Jónsson, J. Phys. Chem. A **113**, 4468 (2009).
[58] J. B. Rommel, T. P. M. Goumans, and J. Kästner, J. Chem. Theory Comput. **7**, 690 (2011).
[59] J. B. Rommel and J. Kästner, J. Chem. Phys. **134**, 184107 (2011).
[60] M. Kryvohuz, J. Chem. Phys. **134**, 114103 (2011).
[61] S. Coleman, *Aspects of Symmetry* (Cambridge University Press, Cambridge, 1985), Chap. 7.
[62] A. I. Vainshtein, V. I. Zakharov, V. A. Novikov, and M. A. Shifman, Sov. Phys. Usp. **25**, 195 (1982).
[63] V. A. Benderskii, D. E. Makarov, and C. A. Wight, *Chemical Dynamics at Low Temperatures, Advances in Chemical Physics* (Wiley, New York, 1994), Vol. 88.
[64] G. V. Mil'nikov and H. Nakamura, J. Chem. Phys. **115**, 6881 (2001).
[65] G. V. Mil'nikov and H. Nakamura, J. Chem. Phys. **122**, 124311 (2005).
[66] J. O. Richardson and S. C. Althorpe, J. Chem. Phys. **134**, 054109 (2011).
[67] I. R. Craig and D. E. Manolopoulos, J. Chem. Phys. **123**, 034102 (2005).
[68] I. R. Craig and D. E. Manolopoulos, J. Chem. Phys. **122**, 084106 (2005).
[69] T. F. Miller III, J. Chem. Phys. **129**, 194502 (2008).
[70] A. Shank, Y. Wang, A. Kaledin, B. J. Braams, and J. M. Bowman, J. Chem. Phys. **130**, 144314 (2009).
[71] Y. Wang, B. C. Shepler, B. J. Braams, and J. M. Bowman, J. Chem. Phys. **131**, 054511 (2009).
[72] We will refer to the minima on the potential energy surface between which tunneling takes place as "wells," to avoid confusing them with the minima on the ring-polymer and linear-polymer surfaces (i.e., the periodic instanton trajectories and kinks).

[73] This treatment can be generalised to the case that there are two or more non-symmetry-related kinks connecting λ to μ. However, unless the weights associated with these kinks are very close, one kink will dominate the other(s) which can thus be ignored. We therefore expect such cases to be rare.

[74] T. R. Dyke, J. Chem. Phys. **66**, 492 (1977).

[75] J. Nocedal, Math. Comput. **35**, 773 (1980).

[76] D. C. Liu and J. Nocedal, Math. Program. **45**, 503 (1989).

[77] D. J. Wales, optim, a program for optimising geometries and calculating pathways, see http://www-wales.ch.cam.ac.uk/software.html.

[78] See supplementary material at http://dx.doi.org/10.1063/1.3640429 for animations of kinks and tables of the calculated energy levels.

[79] D. J. Wales, in *Theory of Atomic and Molecular Clusters*, edited by J. Jellinek, (Springer-Verlag, Heidelberg, Berlin, 1999), p. 86.

[80] D. J. Wales, in *Advances in Molecular Vibrations and Collision Dynamics*, edited by J. M. Bowman, and Z. Bačić, (JAI Press, Stamford, 1998), p. 365.

[81] Note that Ref. 26 employs the notation h_{iv} in place of h_{1i}.

[82] D. J. Wales, J. Am. Chem. Soc. **115**, 11180 (1993).

[83] R. Kumar and J. L. Skinner, J. Phys. Chem. B **112**, 8311 (2008).